




Strong spin-exchange recombination of three weakly interacting ${}^7\text{Li}$ atoms

J.-L. Li ^{*}, T. Secker , P. M. A. Mestrom , and S. J. J. M. F. Kokkelmans
Eindhoven University of Technology, P. O. Box 513, 5600 MB Eindhoven, The Netherlands



(Received 23 July 2021; accepted 9 February 2022; published 9 May 2022)

Quantifying the nonuniversal three-body losses in ultracold atomic gases has been a long-standing problem. We go beyond earlier approaches to solve this problem by using a model that includes realistic pairwise interaction potentials and the exact three-atom spin structure. With this model we can successfully explain experimental observations for weakly interacting ${}^7\text{Li}$ and ${}^{87}\text{Rb}$ atoms. Capturing the exact spin structure, we are able to reveal a strong three-body spin-exchange recombination mechanism. In addition, we predict a regime of low three-body recombination rate in the ${}^7\text{Li}$ system that is advantageous for a variety of many-body experiments. This work opens avenues to study spin-involved few-body processes in quantum gases.

DOI: [10.1103/PhysRevResearch.4.023103](https://doi.org/10.1103/PhysRevResearch.4.023103)

I. INTRODUCTION

Three-body recombination (TBR), the process in which three free particles collide to form a two-body molecule whose binding energy is kinetically distributed among the molecule and free particle, ubiquitously occurs in a vast variety of systems in diverse research fields including astrophysics [1–3], chemistry [4–6], ultracold plasmas [7–9] and ultracold atomic systems [10–28]. In trapped ultracold atomic clouds, for instance, this exothermic process usually causes heating and atom loss, and therefore limits the lifetime and density of Bose-Einstein condensates (BECs) [10,11]. In addition, this loss puts restrictions on the quantum sensitivity of BECs for precision measurements [12], the persistent current of atomtronic circuits [13], and the stability of quantum droplets [14–18]. However, TBR can also be used as a tool to probe Efimov physics [19] and three-body correlations [20–22], cool and even purify ultracold ensembles [23,24], and generate effective three-body interactions [25–27]. The atom loss can be affected by the trap and many-body environment in experimental realizations, making it difficult to determine the TBR rate [22,28]. While in the strong interaction regime the TBR rate is successfully described by universal formulas [29,30], quantifying the TBR rate in weakly interacting atomic gases remains a huge challenge and a numerical approach for it is highly desirable.

TBR occurring in weakly interacting ultracold atomic gases is also a good candidate for understanding fundamental chemistry, given that the reactants can be prepared in a full quantum regime with extremely high control over all external and internal degrees of freedom [31–33]. In addition, experimental milestones of detecting the products have been achieved in the past few years by combining hybrid

atom-ion traps and resonance-enhanced multiphoton ionization techniques [34–36]. This leads to identifying the entire chemical reaction pathway of TBR on the level of full quantum state-to-state resolution regarding the electronic, vibrational, rotational, hyperfine, and even magnetic quantum numbers. In these experiments [34–36], several propensities in TBR processes, such as two atoms conserving their total parity, total spin, and magnetic projection of total spin when forming weakly bound molecular products, are established for ${}^{87}\text{Rb}$ atoms and also explained using the hypothesis that the third atom does not flip its internal spin. Although frequently implemented in previous works for enabling three-body calculations [37–40], this hypothesis may not be generally valid, as is indicated in Ref. [41] for strongly interacting ${}^{39}\text{K}$ atoms. Therefore, whether the hypothesis and the propensities established in the ${}^{87}\text{Rb}$ system are applicable for other species remains an open question.

In this work we investigate the TBR process for weakly interacting ultracold ${}^7\text{Li}$ and ${}^{87}\text{Rb}$ atoms in an external magnetic field using a multichannel framework. We successfully quantify the TBR rate and, for ${}^7\text{Li}$, identify two dominant recombination pathways. One pathway involves spin exchange between the created molecule and the remaining free atom, demonstrating the violation of the aforementioned hypothesis. The rest of the paper is organized as follows: Section II briefly introduces the spin models employed in our three-body calculations. In Sec. III we investigate the TBR process of ${}^7\text{Li}$ atoms in the vicinity of a zero crossing of two-body scattering length at $B = 850$ G and analyze the origin of a strong spin-exchange recombination mechanism in this regime. For comparison, the TBR process of ${}^7\text{Li}$ atoms near a different zero crossing at $B = 578$ G and that of ${}^{87}\text{Rb}$ atoms at $B = 1$ G are studied in Sec. IV. A conclusion is drawn in Sec. V.

II. SPIN MODELS

We follow Ref. [41] to write down the Hamiltonian H_0 , describing three alkali-metal atoms at infinite separation in an external magnetic field B as

$$H_0 = \sum_{\sigma_1\sigma_2\sigma_3} (T + E_{\sigma_1} + E_{\sigma_2} + E_{\sigma_3}) |\sigma_1\sigma_2\sigma_3\rangle \langle\sigma_1\sigma_2\sigma_3|, \quad (1)$$

^{*}Corresponding author: j.li1@tue.nl

Published by the American Physical Society under the terms of the [Creative Commons Attribution 4.0 International](https://creativecommons.org/licenses/by/4.0/) license. Further distribution of this work must maintain attribution to the author(s) and the published article's title, journal citation, and DOI.

where T is the kinetic energy operator, and E_{σ_a} and $|\sigma_a\rangle$ denote the channel energy and the corresponding internal spin state, respectively, of atom a ($a = 1, 2, 3$), which are B dependent. Adiabatically, each state $|\sigma\rangle$ can be unambiguously traced back to a hyperfine state $|f, m_f\rangle$ at zero field or forward to a $|m_s, m_i\rangle$ state at infinite field [42]. Here, f denotes the quantum number of atomic total spin \mathbf{f} summing up the electronic spin \mathbf{s} and nuclear spin \mathbf{i} , and m_f, m_i , and m_s are the corresponding magnetic quantum numbers. Even though commonly (f, m_f) is used for labeling σ , we note that $(m_s, m_i) = \sigma$ is more appropriate in this work given that the considered magnetic fields are high.

In addition to H_0 , we assume that the three atoms interact in a pairwise manner, $V = V_{12} + V_{23} + V_{13}$. The pairwise potential,

$$V_{ab} = V_{ab}^S(r_{ab})\mathcal{P}_{ab}^S + V_{ab}^T(r_{ab})\mathcal{P}_{ab}^T, \quad (2)$$

consists of singlet V_{ab}^S and triplet V_{ab}^T components in the electronic ground configuration of two alkali-metal atoms, where r_{ab} represents the distance between atoms a and b , and \mathcal{P}_{ab}^S (\mathcal{P}_{ab}^T) describes the projector on the electronic singlet (triplet) state of pair (a, b) . We use realistic molecular potentials for V_{ab}^S and V_{ab}^T in this work. We refer to the interaction model in Eq. (2) as the full multichannel spin (FMS) model. Several approximations can be made for simplifying the three-body calculation by restricting the way the atoms interact with each other. One frequently used restriction requires the third (spectating) atom to be fixed to the initial spin state for the other two atoms to interact, referred to as the fixed spectating spin (FSS) model in Ref. [41]. The pairwise interaction under such restriction is expressed as

$$V_{ab}^{\text{FSS}} = V_{ab}|\sigma_c^{\text{in}}\rangle\langle\sigma_c^{\text{in}}|, \quad (3)$$

where $|\sigma_c^{\text{in}}\rangle$ denotes the initial spin state of atom c , and $(a, b, c) = (1, 2, 3), (2, 3, 1),$ or $(3, 1, 2)$. We also construct an optimized spin (OPS) model via

$$V_{ab}^{\text{OPS}} = \sum_{\sigma_c \in \mathcal{D}_c} V_{ab}|\sigma_c\rangle\langle\sigma_c|, \quad (4)$$

where \mathcal{D}_c represents the spin states of atom c that play a dominant role in the collision. It is apparent that the OPS model is equivalent to the FSS model when $\mathcal{D}_c \rightarrow \{\sigma_c^{\text{in}}\}$ and to the FMS model when \mathcal{D}_c includes all single-particle spin states.

Once the spin model is given, we use the Alt-Grassberger-Sandhas (AGS) equation [43] to calculate the partial TBR rate K_3^d for the decay process into a specific atom-molecule channel at zero collisional energy, see Appendix A. Here d labels both the molecule and the corresponding decay channel. The total rate, $K_3 = \sum_d K_3^d$, therefore sums up all partial contributions. We define K_3 such that $dn/dt = -\frac{1}{2}K_3n^3$, where n denotes the density of the atomic gas. This definition is consistent with those in Refs. [41, 44–46], while it differs from that in Ref. [47] by a factor of 2. In our calculations we truncate the molecular orbital angular momentum quantum number l up to l_{max} and implement a cutoff on the relative momentum between the atom and the molecule, see Appendix A.

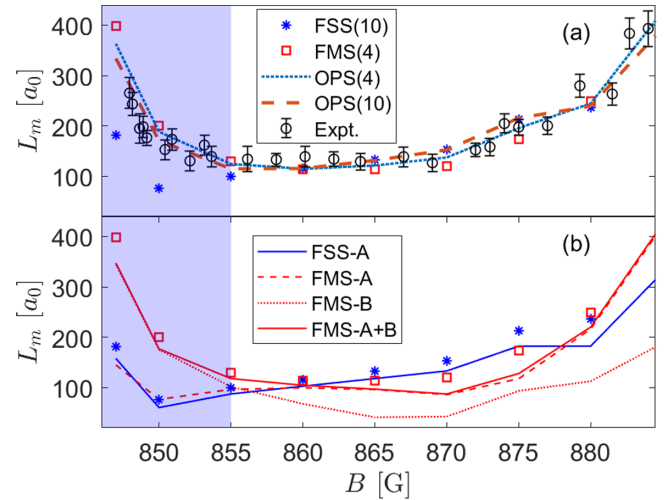


FIG. 1. (a) Three-body recombination length in units of the Bohr radius a_0 for ${}^7\text{Li}$ in the $|m_s = -1/2, m_i = 1/2\rangle$ state. The stars denote the result from the FSS model with $l_{\text{max}} = 10$, while the squares denote the results of the FMS model with $l_{\text{max}} = 4$. The dotted and dashed lines correspond to the calculations using the OPS model with $l_{\text{max}} = 4$ and 10 , respectively. The experimental data at $2.5 \mu\text{K}$ are taken from Ref. [47]. (b) The corresponding partial contributions of the decay channels A and B in the FSS ($l_{\text{max}} = 10$) and FMS ($l_{\text{max}} = 4$) calculations. The stars and squares represent the same results as in (a). The light purple area indicates the strong three-body spin-exchange regime.

III. STRONG SPIN-EXCHANGE TBR

We investigate a system of three ${}^7\text{Li}$ atoms at zero energy initially prepared in the same $|m_s = -1/2, m_i = 1/2\rangle$ state, which corresponds to $|f = 1, m_f = 0\rangle$ in conventional notation. We study the system in an external magnetic field varied between 847 and 885 G, covering a zero crossing of the two-body s -wave scattering length at $B = 850$ G, where experimental data for the TBR rate are reported in Ref. [47]. The singlet and triplet potentials are taken from Ref. [48]. For comparison, we follow Ref. [47] to define the recombination length L_m via

$$K_3 = 328.2 \frac{\hbar}{m} L_m^4, \quad (5)$$

where m denotes the mass of the atom.

Figure 1(a) compares our results to the experimental measurement in Ref. [47]. The result of the FMS calculation with $l_{\text{max}} = 4$ is in good agreement with the experimental results at the considered magnetic fields. However, that of the FSS calculation with $l_{\text{max}} = 10$ only agrees with experiment for $B \gtrsim 860$ G but deviates from the experimental measurement for $B \lesssim 860$ G. The difference in performance between the two approaches does not result from the truncation of the quantum number l , since our additional FSS calculation with $l_{\text{max}} = 4$ leads to only a small shift compared to that with $l_{\text{max}} = 10$, not shown in Fig. 1(a) though. Therefore we attribute the invalidity of the FSS model to its incapability to represent some important three-body channels.

By analyzing our FMS result, we find two dominant product channels, which together contribute more than 50% to the

total TBR rate among more than 300 involved products in our model. We identify that one dominant product channel (decay channel A) consists of the energetically shallowest s -wave molecule with a projection quantum number of total two-body spin $M_{2b} = m_{s_a} + m_{i_a} + m_{s_b} + m_{i_b} = 0$ plus a free atom in its initial $|m_{s_c} = -1/2, m_{i_c} = 1/2\rangle$ spin state. This decay channel is included in the FSS model, and the corresponding contributions to the recombination length are similar in both the FSS and FMS calculations as shown in Fig. 1(b). However, the other dominant product channel (decay channel B) consisting of the shallowest s -wave molecule with $M_{2b} = -1$ plus a free atom in the $|m_{s_c} = -1/2, m_{i_c} = 3/2\rangle$ state is not represented in the FSS model. The spin-exchange recombination to decay channel B becomes increasingly important with decreasing magnetic field at $B \lesssim 860$ G and ultimately dominates over that to decay channel A when $B \lesssim 855$ G, leading to a rapid enhancement of the loss rate. Moreover, its contribution matches very well with the deviation between the FSS calculation and the measurement at $B \lesssim 860$ G.

Allowing the third atom to switch from its initial $|m_{s_c} = -1/2, m_{i_c} = 1/2\rangle$ to the $|m_{s_c} = -1/2, m_{i_c} = 3/2\rangle$ spin state, we arrive at an OPS model with $\mathcal{D}_c = \{(-1/2, 1/2), (-1/2, 3/2)\}$. This OPS model gives results consistent with the measurement, when we truncate the molecular orbital angular momentum quantum number l at $l_{\max} = 4$ and 10. The results are also in line with the values we calculated with the FMS model, demonstrating again that the truncation of l has a minor influence on our calculation.

In Ref. [47], the enhancement of the TBR rate at $B \lesssim 855$ G is suggested to be governed by a two-body length scale L'_e that is determined by the two-body scattering length and effective range parameter. In contrast, our analysis demonstrates that it originates from a single specific atom-molecule product channel coupled to the three-body incoming state via the spin-exchange recombination mechanism. In general, the two-body quantity L'_e is not able to describe this three-body spin-exchange process. It remains an open question why L'_e works beyond its capacity to explain the TBR rate qualitatively [47].

The three-body channels with $|m_{s_c} = -1/2, m_{i_c} = 3/2\rangle$ become important in the present calculation because their small energy separations to the incoming threshold lead to large multichannel couplings, see Appendix B. However, the observed effect that three ${}^7\text{Li}$ atoms recombine predominantly into decay channel B seems counterintuitive at first glance, since decay channel A is less separated from the three-body incoming threshold than decay channel B in the considered magnetic field regime, see Appendix C. To explain the strong recombination into decay channel B, we use an approach similar to that in Ref. [35], in which the TBR rate to a specific decay channel is explained by the overlap of the product molecule state and a zero energy scattering state of two atoms forming that molecule. However, the original treatment of Ref. [35] is based on the hypothesis that the third atom does not flip its internal spin during the TBR process and cannot describe the recombination process into decay channel B. Therefore we extend this treatment by taking into account the interaction with the third atom and the exact three-body spin structure and study the overlap $\mathcal{O}_d = \alpha \langle \psi_d | (P_+ + P_-) V_\alpha | \psi_{\text{scat}} \rangle_\alpha$, see Appendix D. We use $\alpha = (a, b)$ to label

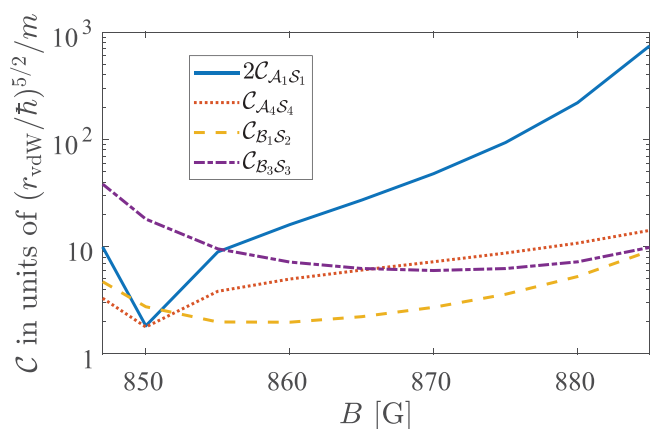


FIG. 2. Components of \mathcal{O}_A and \mathcal{O}_B as a function of magnetic field. Here r_{vdW} denotes the characteristic length scale for the van der Waals interaction between two atoms [42].

the pair (a, b) that forms the molecule d . $|\psi_d\rangle_\alpha$ and $|\psi_{\text{scat}}\rangle_\alpha$ denote the state of molecule d plus a free atom and that of a zero-energy scattering complex of the pair (a, b) plus a free atom, respectively [49]. The interaction term $(P_+ + P_-)V_\alpha$ that couples $|\psi_{\text{scat}}\rangle_\alpha$ and $|\psi_d\rangle_\alpha$ is derived from a perturbative analysis of the AGS equation, see Appendix D. P_+ and P_- denote the cyclic and anticyclic permutation operators, respectively. We use \mathcal{O}_d to explain the dominances of decay channels A and B as it captures the overall trend and relative magnitude of the TBR rates at the considered magnetic fields, see Appendix D.

The overlaps \mathcal{O}_A and \mathcal{O}_B are written as

$$\mathcal{O}_d = 2 \sum_{\sigma_{2b}^d, \sigma_{2b}^{\text{scat}}} C_{\sigma_{2b}^d \sigma_{2b}^{\text{scat}}} \langle \sigma_{2b}^d \sigma_c^d | P_+^s | \sigma_{2b}^{\text{scat}} \sigma_c^{\text{in}} \rangle, d = A, B, \quad (6)$$

where $C_{\sigma_{2b}^d \sigma_{2b}^{\text{scat}}} \equiv \alpha \langle \psi_d | P_+^c | \sigma_{2b}^d \sigma_c^d \rangle \langle \sigma_{2b}^{\text{scat}} \sigma_c^{\text{in}} | V_\alpha | \psi_{\text{scat}} \rangle_\alpha$ represents the spatial part of \mathcal{O}_d , which can be simplified as $C_{\sigma_{2b}^d \sigma_{2b}^{\text{scat}}} = \langle \phi_d | \frac{1}{2} q_d, \sigma_{2b}^d \rangle \langle q_d, \sigma_{2b}^{\text{scat}} | V_\alpha | \phi_{\text{scat}} \rangle_\alpha$, see Appendix D. We use P_+^s and P_+^c to denote the permutation operator P_+ acting only on the spin and coordinate space and $\sigma_{2b} = (m_{s_a}, m_{i_a}; m_{s_b}, m_{i_b})$ for the spin state of the pair (a, b) . We assume that $|\sigma_{2b}\rangle$ is properly symmetrized as in Ref. [41]. Here ϕ_d and ϕ_{scat} represent the radial wave functions of molecule d and the two-body scattering state, respectively. Furthermore, q_d denotes the magnitude of the relative momentum between the free atom and molecule d .

We find that the field-independent spin coupling matrix $\langle \sigma_{2b}^d \sigma_c^d | P_+^s | \sigma_{2b}^{\text{scat}} \sigma_c^{\text{in}} \rangle$ picks out only a few specific elements of \mathcal{C} that contribute to the overlap \mathcal{O}_d . For both decay channels A and B, there are only two contributions of which the corresponding spin states and spin coupling matrix elements are listed in Table I. Implementing the results of Table I into Eq. (6), we get

$$\begin{aligned} \mathcal{O}_A &= 2\mathcal{C}_{A_1 S_1} + \mathcal{C}_{A_4 S_4}, \\ \mathcal{O}_B &= \mathcal{C}_{B_1 S_2} + \mathcal{C}_{B_3 S_3}. \end{aligned} \quad (7)$$

The above expression shows explicitly that the interplay between two specific elements of the spatial part matrix \mathcal{C} determines the overlap \mathcal{O}_d . Figure 2 shows that $2\mathcal{C}_{A_1 S_1}$ and $\mathcal{C}_{B_3 S_3}$ are the most significant contributions at $B \gtrsim 855$ G and

TABLE I. Nonzero elements of $\langle \sigma_{2b}^d \sigma_c^d | P_+^s | \sigma_{2b}^{\text{scat}} \sigma_c^{\text{in}} \rangle$ and the corresponding spin states for decay channels A and B. We use $\sigma_{2b}^A = \{\mathcal{A}_1, \mathcal{A}_2, \dots, \mathcal{A}_8\}$, $\sigma_{2b}^B = \{\mathcal{B}_1, \mathcal{B}_2, \dots, \mathcal{B}_6\}$, and $\sigma_{2b}^{\text{scat}} = \{\mathcal{S}_1, \mathcal{S}_2, \dots, \mathcal{S}_8\}$ to label these two-body spin states in the order of increasing two-body channel energy. Note that $\sigma_c^{\text{in}} = (-1/2, 1/2)$ in all cases.

d	σ_c^d	σ_{2b}^d	$\sigma_{2b}^{\text{scat}}$	$\langle \sigma_{2b}^d \sigma_c^d P_+^s \sigma_{2b}^{\text{scat}} \sigma_c^{\text{in}} \rangle$
A	$(-1/2, 1/2)$	$\mathcal{A}_1 = (-1/2, 1/2; -1/2, 1/2)$	$\mathcal{S}_1 = (-1/2, 1/2; -1/2, 1/2)$	1
A	$(-1/2, 1/2)$	$\mathcal{A}_4 = (-1/2, 1/2; 1/2, -1/2)$	$\mathcal{S}_4 = (-1/2, 1/2; 1/2, -1/2)$	1/2
B	$(-1/2, 3/2)$	$\mathcal{B}_1 = (-1/2, -1/2; -1/2, 1/2)$	$\mathcal{S}_2 = (-1/2, -1/2; -1/2, 3/2)$	1/2
B	$(-1/2, 3/2)$	$\mathcal{B}_3 = (1/2, -3/2; -1/2, 1/2)$	$\mathcal{S}_3 = (1/2, -3/2; -1/2, 3/2)$	1/2

$B \lesssim 855$ G, respectively. The enhanced behavior of $2C_{\mathcal{A}_1, \mathcal{S}_1}$ and $C_{\mathcal{B}_3, \mathcal{S}_3}$ thus explains the dominance of decay channels A and B in each magnetic field regime. We find that these enhancements originate from the influence of the Feshbach resonance at $B = 894$ G on the molecular wave function ϕ_A and that of the Feshbach resonance at $B = 845$ G on the two-body scattering wave function ϕ_{scat} , respectively, see Appendix E.

IV. LOWER FIELD ZERO CROSSING AND COMPARISON TO ^{87}Rb

For comparison, we investigate the TBR rate near a different zero crossing of the two-body scattering length at $B = 578$ G in the same spin state of ^7Li [51]. Table II shows that K_3 at $B = 850$ G is higher by two orders of magnitude than that at $B = 578$ G, where the comparable values of K_3 predicted by the FSS and FMS models indicate no strong spin-exchange process. We note that decay channel B becomes less important at $B = 578$ G, see Appendix D. However, the scenario of ^7Li at $B = 578$ G is still in contrast with the ^{87}Rb system, where the FSS and FMS calculations yield nearly identical results. Therefore we conclude that the model with the fixed spectating atom's spin state works very well for ^{87}Rb at low magnetic fields but not for ^7Li . In general, the TBR rates from our calculation agree with experimental values [20,47] within a factor of 2 or 3. The deviation could come from our numerical truncations or from the experimental uncertainty in the number of atoms. For instance, by implementing a larger $l_{\text{max}} = 10$ with the OPS model we get $K_3 = 2.0 \times 10^{-26} \text{ cm}^6/\text{s}$ at $B = 850$ G, which agrees better with the experimentally measured value $1.3(0.4) \times 10^{-26} \text{ cm}^6/\text{s}$ [47].

Our prediction of low TBR rate suggests that ^7Li at $B \approx 578$ G is a good candidate for the first realization of quantum gas purification experiments via three-body loss [24] and the creation of big time crystals [52]. Other interesting

TABLE II. K_3 from the FMS and FSS models for ^7Li at $B = 850$ G (H) and $B = 578$ G (L), and for ^{87}Rb in the $|f = 1, m_f = -1\rangle$ state at $B = 1$ G. In these calculations we take $l_{\text{max}} = 4$ for ^7Li and $l_{\text{max}} = 10$ for ^{87}Rb . The numbers are presented in units of cm^6/s . The singlet and triplet potentials for ^{87}Rb are taken from Ref. [50].

Atom	FSS	FMS	Expt.
$^7\text{Li(H)}$	1.0×10^{-27}	3.8×10^{-26}	$1.3(0.4) \times 10^{-26}$ [47]
$^7\text{Li(L)}$	1.7×10^{-28}	1.2×10^{-28}	$< 2.3 \times 10^{-27}$ [47]
^{87}Rb	4.0×10^{-29}	4.0×10^{-29}	$8.6(3.6) \times 10^{-29}$ [20]

phenomena like the matter wave bright soliton [53–56] and the weak collapse of a Bose-Einstein condensate [57], which have been experimentally studied, can also be investigated in this specific case, where an extremely small slope $0.01 a_0/\text{G}$ of the two-body scattering length to magnetic field leads to easy and precise control of the required weak attractive interaction.

V. CONCLUSION

We have studied the three-body recombination process of ultracold ^7Li atoms near two zero crossings of the two-body scattering length at $B = 850$ G and 578 G. In the vicinity of 850 G, we get a good agreement with the measured recombination rate and reveal a prominent spin-exchange three-body recombination pathway requiring one atom to flip its nuclear spin when the other two colliding atoms form a molecule. We attribute the prominence of this pathway to the influence of the Feshbach resonance at $B = 845$ G on the two-body scattering wave function. The strong spin-exchange effect increases the recombination rate by about two orders of magnitude compared to our results around 578 G in the same spin state. Our approach can also be applied to other species to explore the complicated but important multichannel three-body recombination process and to analyze the rich interplay between the translational, vibrational, rotational, electronic spin, and nuclear spin degrees of freedom.

ACKNOWLEDGMENTS

We thank Lev Khaykovich, Denise Ahmed-Braun, Victor Colussi, Gijs Groeneveld, and Silvia Musolino for discussions. This research is financially supported by the Netherlands Organisation for Scientific Research (NWO) under Grant No. 680-47-623.

APPENDIX A: AGS EQUATION AND TBR RATE

We solve the AGS equation in momentum space [41,45,46,58],

$$U_{\alpha 0}(z) = \frac{1}{3} G_0^{-1}(z) [1 + P_+ + P_-] + [P_+ + P_-] \mathcal{T}_\alpha(z) G_0(z) U_{\alpha 0}(z), \quad (\text{A1})$$

via a numerical approach combining the separable expansion method and the two-body mapped grid technique [41,46]. Here $G_0 = (z - H_0)^{-1}$ is the free Green's operator, and $\mathcal{T}_\alpha = (1 - V_\alpha G_0(z))^{-1} V_\alpha$ represents the generalized two-body transition operator for the pair $\alpha = (a, b)$. P_+ and P_- denote the cyclic and anticyclic permutation operators, respectively. The three-body transition operator $U_{\alpha 0}$, whose elements describe

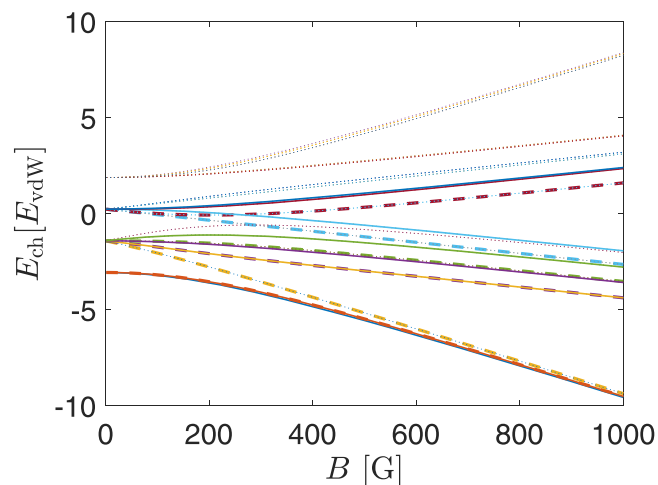


FIG. 3. Channel energy E_{ch} in units of $E_{\text{vdW}} = \hbar^2/(mr_{\text{vdW}}^2)$ of three ${}^7\text{Li}$ atoms with $M_{\text{tot}} = 0$. The solid and dashed lines represent the three-body channels with $\sigma_c = (-1/2, 1/2)$ and $(-1/2, 3/2)$, respectively. The dotted lines correspond to other σ_c . The incoming three-body channel is the lowest one.

the transition probabilities from the initial free-atom state to product states of a dimer plus a free atom, is closely related to the TBR rate K_3 . In this paper we define the partial recombination rate K_3^d to each specific molecular product d as [41,45,46,58]

$$K_3^d = \frac{24\pi m}{\hbar} (2\pi\hbar)^6 q_d |\langle \psi_d | U_{\alpha 0}(z) | \psi_{\text{in}} \rangle|^2, \quad (\text{A2})$$

where $|\psi_{\text{in}}\rangle$ and $|\psi_d\rangle$ represent the initial and product states, respectively. q_d is the magnitude of the momentum of the free atom relative to the center of mass of molecule d . In our calculations, we take the zero energy limit $z \rightarrow 0$ from the upper half of the complex energy plane and therefore fix the total orbital angular momentum quantum number $J = 0$. The projection quantum number of the total spin angular momentum $M_{\text{tot}} = \sum_a m_{s_a} + \sum_a m_{i_a}$ ($a = 1, 2$, and 3) should also be fixed during the scattering process, $M_{\text{tot}} = 0$ in the present case. We also implement truncations l_{max} on the orbital angular momentum quantum number l related to the relative movement of the atoms constituting the molecule and q_{max} on the magnitude of the momentum q of the third atom relative to the molecule's center of mass. In particular, $q_{\text{max}} = 20 \hbar/r_{\text{vdW}}$ is used throughout the entire paper, and l_{max} is stated explicitly when the results are presented in the main text. It is worth noting that the sufficiency of $q_{\text{max}} = 20 \hbar/r_{\text{vdW}}$ is demonstrated for addressing the three-body parameter in Refs. [41,46] and additionally checked for our present study by comparing to a larger cutoff $q_{\text{max}} = 40 \hbar/r_{\text{vdW}}$. For more details about our numerical approach, we refer the reader to Refs. [41,46].

APPENDIX B: THREE-BODY CHANNEL ENERGY

Figure 3 shows the three-body channel energy $E_{\text{ch}} = E_a + E_b + E_c$ with $M_{\text{tot}} = 0$ for ${}^7\text{Li}$ atoms. One can see that the channel energy separations are in general smaller than those for ${}^{39}\text{K}$ atoms [41]. In particular, for those with $\sigma_c = (-1/2, 3/2)$, the two lowest channels are extremely close, with energy separations less than $0.25 E_{\text{vdW}}$, to the three-body

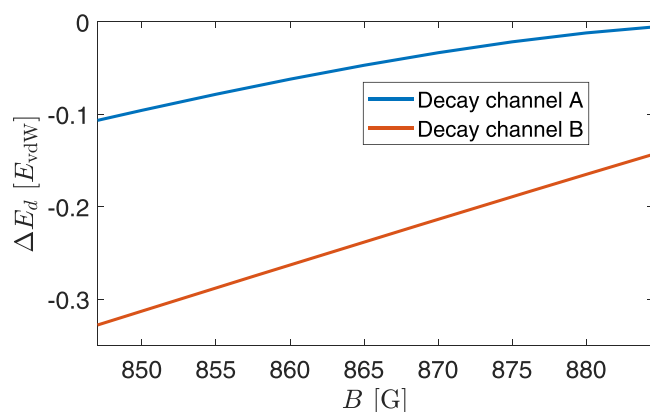


FIG. 4. Energy separations ΔE_d of decay channels A and B from the incoming threshold as a function of magnetic field.

incoming channel when $B > 800$ G. According to the analysis in Ref. [41], this can lead to strong multichannel couplings to the incoming channel.

APPENDIX C: ASYMPTOTIC ENERGY OF DECAY CHANNELS A AND B

To illustrate the energy separations of the product channels from the incoming channel, we calculate $\Delta E_d = E_{2b}^d + E_{\sigma_c^d} - E_{\sigma_a^{\text{in}}} - E_{\sigma_b^{\text{in}}} - E_{\sigma_c^{\text{in}}}$ for $d = A$ or B , where E_{2b}^d denotes the energy level of molecule d and $E_{\sigma_c^d}$ represents the corresponding shift due to the third atom. In the zero energy limit considered in this work, ΔE_d is simply connected to q_d via $\Delta E_d = -3q_d^2/4m$. Figure 4 shows the energy levels of both decay channels are shifted towards the incoming threshold with the increase of the magnetic field and $|\Delta E_A|$ persists to be smaller than $|\Delta E_B|$ in the considered magnetic field regime. These energy separations explain the dominance of decay channel A at $B \gtrsim 860$ G. However, it is in contrast with our observation that K_3^B is much larger than K_3^A at $B \lesssim 855$ G.

APPENDIX D: TBR RATE FROM \mathcal{O}_d

To get the expression of \mathcal{O}_d in the main text, we rewrite Eq. (A1) as

$$U_{\alpha 0}(z) = \sum_{n=0}^{\infty} U_{\alpha 0}^{(n)}(z) \quad (\text{D1})$$

with

$$U_{\alpha 0}^{(n)}(z) = \{[P_+ + P_-] \mathcal{T}_{\alpha}(z) G_0(z)\}^n \frac{1}{3} G_0^{-1}(z) [1 + P_+ + P_-]. \quad (\text{D2})$$

Since ${}_{\alpha} \langle \psi_d | U_{\alpha 0}^{(0)}(z) | \psi_{\text{in}} \rangle$ vanishes at zero energy, we look into the next order term $U_{\alpha 0}^{(1)}(z)$. The initial free-atom state is taken as $|\psi_{\text{in}}\rangle = |\mathbf{p} = \mathbf{0}, \mathbf{q} = \mathbf{0}\rangle |\sigma_a^{\text{in}} \sigma_b^{\text{in}} \sigma_c^{\text{in}}\rangle$, where \mathbf{p} and \mathbf{q} are Jacobi momenta corresponding to the relative motion between two atoms and that of the third atom to the center of mass of them, respectively. $|\psi_{\text{in}}\rangle$ is fully symmetric so that

$$U_{\alpha 0}^{(1)}(z) |\psi_{\text{in}}\rangle = [P_+ + P_-] \mathcal{T}_{\alpha}(z) |\psi_{\text{in}}\rangle. \quad (\text{D3})$$

We implement the partial wave expansion and switch from the plane-wave basis $|\mathbf{p}, \mathbf{q}\rangle$ to $|p, q\rangle |lLM_J\rangle$, where l and L

are partial wave quantum numbers corresponding to \mathbf{p} and \mathbf{q} , respectively. The initial and product states can then be expressed as $|\psi_{\text{in}}\rangle = \frac{1}{4\pi}|p=0, q=0\rangle|0000\rangle|\sigma_a^{\text{in}}\sigma_b^{\text{in}}\sigma_c^{\text{in}}\rangle$ and $|\psi_d\rangle_\alpha = |\phi_d, q_d\rangle_\alpha |l_d l_d 00\rangle |\sigma_c^d\rangle$, where ϕ_d denotes the radial wave function of molecule d . We define $|\psi_{\text{scat}}\rangle_\alpha \equiv |\phi_{\text{scat}}, q =$

$0\rangle_\alpha |0000\rangle |\sigma_c^{\text{in}}\rangle$ to describe the state of a scattering complex plus a free atom, where ϕ_{scat} is the radial two-body scattering wave function at zero energy. Using these states and Eq. (D3), we get

$$\begin{aligned} \alpha \langle \psi_d | U_{\alpha 0}^{(1)}(0) | \psi_{\text{in}} \rangle &= \frac{1}{4\pi} \alpha \langle \psi_d | [P_+ + P_-] \mathcal{T}_\alpha(0) | p=0, q=0 \rangle | 0000 \rangle | \sigma_a^{\text{in}} \sigma_b^{\text{in}} \sigma_c^{\text{in}} \rangle \\ &= \frac{1}{4\pi} \alpha \langle \psi_d | [P_+ + P_-] V_\alpha | \phi_{\text{scat}}, q=0 \rangle | 0000 \rangle | \sigma_c^{\text{in}} \rangle \\ &= \frac{1}{4\pi} \mathcal{O}_d \end{aligned} \quad (\text{D4})$$

with

$$\begin{aligned} \mathcal{O}_d &= \alpha \langle \psi_d | [P_+ + P_-] V_\alpha | \psi_{\text{scat}} \rangle_\alpha \\ &= 2 \sum_{\sigma_{2b}^d, \sigma_{2b}^{\text{scat}}} \alpha \langle \psi_d | P_+^c | \sigma_{2b}^d \sigma_c^d \rangle \langle \sigma_{2b}^{\text{scat}} \sigma_c^{\text{in}} | V_\alpha | \psi_{\text{scat}} \rangle_\alpha \langle \sigma_{2b}^d \sigma_c^d | P_+^s | \sigma_{2b}^{\text{scat}} \sigma_c^{\text{in}} \rangle \\ &= 2 \sum_{\sigma_{2b}^d, \sigma_{2b}^{\text{scat}}} \int d\mathbf{q}' \int d\mathbf{q}'' \alpha \langle \psi_d | \mathbf{q}'' + \frac{1}{2}\mathbf{q}', \mathbf{q}' \rangle | \sigma_{2b}^d \sigma_c^d \rangle \langle \sigma_{2b}^{\text{scat}} \sigma_c^{\text{in}} | \left\langle -\mathbf{q}' - \frac{1}{2}\mathbf{q}'', \mathbf{q}'' \right\rangle V_\alpha | \psi_{\text{scat}} \rangle_\alpha \langle \sigma_{2b}^d \sigma_c^d | P_+^s | \sigma_{2b}^{\text{scat}} \sigma_c^{\text{in}} \rangle \\ &= 2\sqrt{2l_d+1} \sum_{\sigma_{2b}^d, \sigma_{2b}^{\text{scat}}} \langle \sigma_c^d | \alpha \langle \phi_d | \frac{1}{2}q_d, \sigma_{2b}^d \sigma_c^d \rangle \langle q_d, \sigma_{2b}^{\text{scat}} \sigma_c^{\text{in}} | V_\alpha | \phi_{\text{scat}} \rangle_\alpha | \sigma_c^{\text{in}} \rangle \langle \sigma_{2b}^d \sigma_c^d | P_+^s | \sigma_{2b}^{\text{scat}} \sigma_c^{\text{in}} \rangle \\ &= 2\sqrt{2l_d+1} \sum_{\sigma_{2b}^d, \sigma_{2b}^{\text{scat}}} \alpha \langle \phi_d | \frac{1}{2}q_d, \sigma_{2b}^d \rangle \langle q_d, \sigma_{2b}^{\text{scat}} | V_\alpha | \phi_{\text{scat}} \rangle_\alpha \langle \sigma_{2b}^d \sigma_c^d | P_+^s | \sigma_{2b}^{\text{scat}} \sigma_c^{\text{in}} \rangle \\ &= 2\sqrt{2l_d+1} \sum_{\sigma_{2b}^d, \sigma_{2b}^{\text{scat}}} \phi_{2b}^{\sigma_{2b}^d} \left(\frac{1}{2}q_d \right) t_h^{\sigma_{2b}^{\text{scat}}}(q_d) \langle \sigma_{2b}^d \sigma_c^d | P_+^s | \sigma_{2b}^{\text{scat}} \sigma_c^{\text{in}} \rangle, \end{aligned} \quad (\text{D5})$$

where

$$t_h^{\sigma_{2b}^{\text{scat}}}(q_d) = \langle q_d, \sigma_{2b}^{\text{scat}} | V_\alpha | \phi_{\text{scat}} \rangle_\alpha = \langle \sigma_{2b}^{\text{scat}} | \langle p=q_d | t_\alpha^{l=0}(z_{2b}=0) | p_z=0 \rangle | \sigma_a^{\text{in}} \sigma_b^{\text{in}} \rangle \quad (\text{D6})$$

is an element of the two-body s -wave t matrix $t^{l=0}$ at two-body energy $z_{2b} = p_z^2/m = 0$ with one momentum fixed on the energy shell, which is commonly referred to as the half-shell t matrix in nuclear physics [59,60]. The expression of Eq. (6) in the main text is obtained by filling in $l_d = 0$ for $d = A$ or B in Eq. (D5).

Figure 5(a) shows that the TBR rates calculated from \mathcal{O}_d follow the overall trend of those given by the FMS calculation

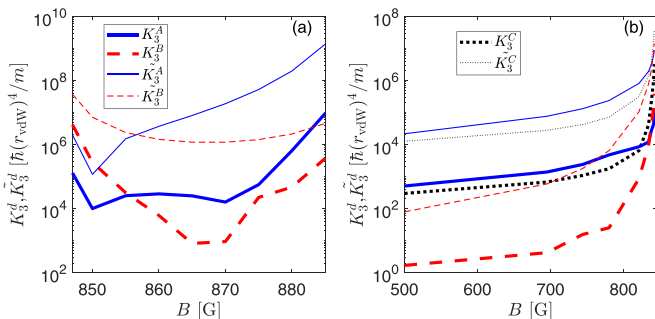


FIG. 5. The TBR rates for decay channels A, B, and C calculated from $U_{\alpha 0}$ by using the FMS model with $l_{\text{max}} = 4$ (K_3^d) or from $U_{\alpha 0}^{(1)}$ by using \mathcal{O}_d (\tilde{K}_3^d).

with $l_{\text{max}} = 4$ in our considered magnetic field regime. The main feature that three free atoms recombine predominantly into decay channel B at $B \lesssim 855$ G and into decay channel A at $B \gtrsim 855$ G is captured by \mathcal{O}_d . Similarly, \mathcal{O}_d captures the overall trend and relative magnitude of the TBR rates near a different zero crossing at $B = 578$ G, as is shown in Fig. 5(b). However, the absolute magnitude of the TBR rates cannot be correctly addressed by \mathcal{O}_d , indicating that our multichannel numerical calculation is indispensable for quantifying the TBR rates. Figure 5(b) also demonstrates that the spin-exchange recombination pathway to decay channel B is strongly suppressed near the zero crossing at $B = 578$ G. We note that decay channel C in Fig. 5(b) corresponds to the new shallow molecule with $M_{2b} = 0$ appearing when the magnetic field decreases over the Feshbach resonance position at $B = 845$ G.

APPENDIX E: ANALYSIS ON $\mathcal{C}_{A_1 S_1}$ AND $\mathcal{C}_{B_3 S_3}$

We have demonstrated in the main text that \mathcal{O}_A is determined by $\mathcal{C}_{A_1 S_1}$ at $B \gtrsim 855$ G and \mathcal{O}_B is determined by $\mathcal{C}_{B_3 S_3}$ at $B \lesssim 855$ G. Now we want to analyze which quantities make these two components the most significant. For that we write

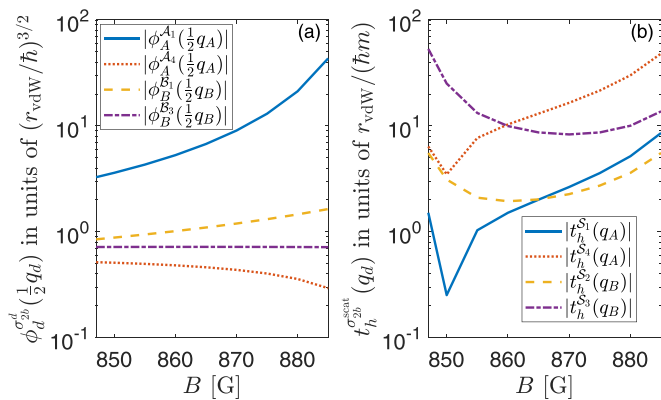


FIG. 6. The molecular wave function evaluated at $\frac{1}{2}q_d$ (a) and half-shell t -matrix evaluated at q_d (b) relevant for the overlaps \mathcal{O}_A and \mathcal{O}_B .

$\mathcal{C}_{\mathcal{A}_1 S_1}$ and $\mathcal{C}_{\mathcal{B}_3 S_3}$ as

$$\begin{aligned}\mathcal{C}_{\mathcal{A}_1 S_1} &= \phi_A^{A_1}(\tfrac{1}{2}q_A)t_h^{S_1}(q_A), \\ \mathcal{C}_{\mathcal{B}_3 S_3} &= \phi_B^{B_3}(\tfrac{1}{2}q_B)t_h^{S_3}(q_A).\end{aligned}\quad (\text{E1})$$

Figure 6(a) shows that the large value of $\mathcal{C}_{\mathcal{A}_1 S_1}$ at $B \gtrsim 855$ G comes from $\phi_A^{A_1}(\frac{1}{2}q_A)$. The increasing behavior of $\phi_A^{A_1}(\frac{1}{2}q_A)$ with the increase of magnetic field can be understood as follows. Molecule A becomes increasingly extended in the \mathcal{A}_1 channel when its energy level is shifted towards the threshold of that channel. Eventually, the energy level of molecule A merges with the threshold of the \mathcal{A}_1 channel at the Feshbach resonance position of $B = 894$ G. As a result, ϕ_A increases the amplitude of its \mathcal{A}_1 component in the large-distance (or equivalently, low-momentum) regime, as is shown in Figs. 7(a)–7(c). In combination with a simultaneously decreasing q_A , this leads to a rapid increase of $\phi_A^{A_1}(\frac{1}{2}q_A)$.

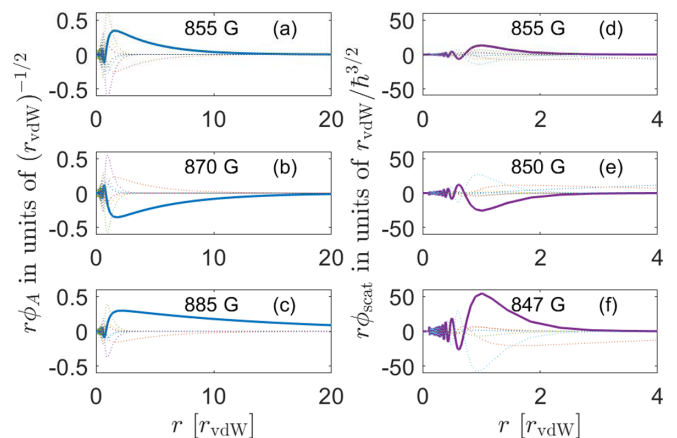


FIG. 7. (a)–(c) Molecular wave function ϕ_A at $B = 855, 870,$ and 885 G. (d)–(f) Two-body scattering wave function ϕ_{scat} at $B = 855, 850,$ and 847 G. The solid lines highlight the $\sigma_{2b}^{A_1}$ component for ϕ_A in (a)–(c) and the $\sigma_{2b}^{B_3}$ component for ϕ_{scat} in (d)–(f).

In contrast, the enhancement of $\mathcal{C}_{\mathcal{B}_3 S_3}$ at $B \lesssim 855$ G with the decreasing magnetic field comes from that of $t_h^{S_3}(q_B)$, as shown in Fig. 6(b). The behavior of $t_h^{S_3}(q_B)$ at $B \lesssim 855$ G can be related to the Feshbach resonance at $B = 845$ G. In the vicinity of this Feshbach resonance, the two-body scattering state $|\phi_{\text{scat}}\rangle$ increases the amplitudes of its closed channel components at short range due to the coupling from the resonant molecular state, as is shown in Figs. 7(d)–7(f). This leads to an enhanced component of the two-body half-shell t matrix in the corresponding closed channels. In the present case, S_3 is one of the closed channels with enhanced components. Therefore $t_h^{S_3}(q_B)$ increases when the magnetic field is tuned towards the Feshbach resonance at $B = 845$ G. Similarly, $t_h^{S_3}(q_B)$ is also enhanced in the vicinity of the Feshbach resonance at $B = 894$ G.

- [1] F. Palla, E. E. Salpeter, and S. W. Stahler, Primordial star formation – The role of molecular hydrogen, *Astrophys. J.* **271**, 632 (1983).
- [2] D. R. Flower and G. J. Harris, Three-body recombination of hydrogen during primordial star formation, *Mon. Not. R. Astron. Soc.* **377**, 705 (2007).
- [3] M. J. Turk, P. Clark, S. C. O. Glover, T. H. Greif, T. Abel, R. Klessen, and V. Bromm, Effects of varying the three-body molecular hydrogen formation rate in primordial STAR FORMATION, *Astrophys. J.* **726**, 55 (2010).
- [4] A. D. Stepukhovich and V. M. Umanskii, Kinetics and mechanism of three-body recombination of atoms and radicals, *Russ. Chem. Rev.* **38**, 590 (1969).
- [5] J. P. Ríos, *An Introduction to Cold and Ultracold Chemistry* (Springer International Publishing, Cham, Switzerland, 2020).
- [6] J. Pérez-Ríos, Cold chemistry: A few-body perspective on impurity physics of a single ion in an ultracold bath, *Mol. Phys.* **119**, e1881637 (2021).
- [7] T. C. Killian, M. J. Lim, S. Kulin, R. Dumke, S. D. Bergeson, and S. L. Rolston, Formation of Rydberg Atoms in an Expanding Ultracold Neutral Plasma, *Phys. Rev. Lett.* **86**, 3759 (2001).
- [8] R. S. Fletcher, X. L. Zhang, and S. L. Rolston, Using Three-Body Recombination to Extract Electron Temperatures of Ultracold Plasmas, *Phys. Rev. Lett.* **99**, 145001 (2007).
- [9] M. Lyon and S. L. Rolston, Ultracold neutral plasmas, *Rep. Prog. Phys.* **80**, 017001 (2016).
- [10] T. Weber, J. Herbig, M. Mark, H.-C. Nägerl, and R. Grimm, Three-Body Recombination at Large Scattering Lengths in an Ultracold Atomic Gas, *Phys. Rev. Lett.* **91**, 123201 (2003).
- [11] C. J. Pethick and H. Smith, *Bose–Einstein Condensation in Dilute Gases*, 2nd ed. (Cambridge University Press, Cambridge, England, 2008).
- [12] D. Rätzel and R. Schützhold, Decay of quantum sensitivity due to three-body loss in Bose-Einstein condensates, *Phys. Rev. A* **103**, 063321 (2021).
- [13] M. Kunimi and I. Danshita, Decay mechanisms of superflow of Bose-Einstein condensates in ring traps, *Phys. Rev. A* **99**, 043613 (2019).
- [14] P. M. A. Mestrom, V. E. Colussi, T. Secker, G. P. Groeneveld, and S. J. J. M. F. Kokkelmans, Van Der Waals Universality Near a Quantum Tricritical Point, *Phys. Rev. Lett.* **124**, 143401 (2020).

- [15] C. R. Cabrera, L. Tanzi, J. Sanz, B. Naylor, P. Thomas, P. Cheiney, and L. Tarruell, Quantum liquid droplets in a mixture of Bose-Einstein condensates, *Science* **359**, 301 (2018).
- [16] P. Cheiney, C. R. Cabrera, J. Sanz, B. Naylor, L. Tanzi, and L. Tarruell, Bright Soliton to Quantum Droplet Transition in a Mixture of Bose-Einstein Condensates, *Phys. Rev. Lett.* **120**, 135301 (2018).
- [17] G. Semeghini, G. Ferioli, L. Masi, C. Mazzinghi, L. Wolswijk, F. Minardi, M. Modugno, G. Modugno, M. Inguscio, and M. Fattori, Self-Bound Quantum Droplets of Atomic Mixtures in Free Space, *Phys. Rev. Lett.* **120**, 235301 (2018).
- [18] F. Böttcher, J.-N. Schmidt, J. Hertkorn, K. S. H. Ng, S. D. Graham, M. Guo, T. Langen, and T. Pfau, New states of matter with fine-tuned interactions: Quantum droplets and dipolar supersolids, *Rep. Prog. Phys.* **84**, 012403 (2021).
- [19] T. Kraemer, M. Mark, P. Waldburger, J. Danzl, C. Chin, B. Engeser, K. Pilch, A. Jaakkola, H.-C. Nägerl, and R. Grimm, Evidence for Efimov quantum states in an ultracold gas of caesium atoms, *Nature (London)* **440**, 315 (2006).
- [20] E. A. Burt, R. W. Ghrist, C. J. Myatt, M. J. Holland, E. A. Cornell, and C. E. Wieman, Coherence, Correlations, and Collisions: What One Learns about Bose-Einstein Condensates from Their Decay, *Phys. Rev. Lett.* **79**, 337 (1997).
- [21] B. L. Tolra, K. M. O'Hara, J. H. Huckans, W. D. Phillips, S. L. Rolston, and J. V. Porto, Observation of Reduced Three-Body Recombination in a Correlated 1D Degenerate Bose Gas, *Phys. Rev. Lett.* **92**, 190401 (2004).
- [22] L. A. Reynolds, E. Schwartz, U. Ebling, M. Weyland, J. Brand, and M. F. Andersen, Direct Measurements of Collisional Dynamics in Cold Atom Triads, *Phys. Rev. Lett.* **124**, 073401 (2020).
- [23] M. Schemmer and I. Bouchoule, Cooling a Bose Gas by Three-Body Losses, *Phys. Rev. Lett.* **121**, 200401 (2018).
- [24] L. H. Dogra, J. A. P. Glidden, T. A. Hilker, C. Eigen, E. A. Cornell, R. P. Smith, and Z. Hadzibabic, Can Three-Body Recombination Purify a Quantum Gas? *Phys. Rev. Lett.* **123**, 020405 (2019).
- [25] A. J. Daley, J. M. Taylor, S. Diehl, M. Baranov, and P. Zoller, Atomic Three-Body Loss as a Dynamical Three-Body Interaction, *Phys. Rev. Lett.* **102**, 040402 (2009).
- [26] A. J. Daley, J. M. Taylor, S. Diehl, M. Baranov, and P. Zoller, Erratum: Atomic Three-Body Loss as a Dynamical Three-Body Interaction [Phys. Rev. Lett. **102**, 040402 (2009)], *Phys. Rev. Lett.* **102**, 179902(E) (2009).
- [27] M. Roncaglia, M. Rizzi, and J. I. Cirac, Pfaffian State Generation by Strong Three-Body Dissipation, *Phys. Rev. Lett.* **104**, 096803 (2010).
- [28] L. A. Zundel, J. M. Wilson, N. Malvania, L. Xia, J.-F. Riou, and D. S. Weiss, Energy-Dependent Three-Body Loss in 1D Bose Gases, *Phys. Rev. Lett.* **122**, 013402 (2019).
- [29] E. Braaten and H.-W. Hammer, Universality in few-body systems with large scattering length, *Phys. Rep.* **428**, 259 (2006).
- [30] J. P. D'Incao, Few-body physics in resonantly interacting ultracold quantum gases, *J. Phys. B: At., Mol. Opt. Phys.* **51**, 043001 (2018).
- [31] N. Balakrishnan, Perspective: Ultracold molecules and the dawn of cold controlled chemistry, *J. Chem. Phys.* **145**, 150901 (2016).
- [32] G. Quéméner and P. S. Julienne, Ultracold molecules under control! *Chem. Rev.* **112**, 4949 (2012).
- [33] C. H. Greene, P. Giannakeas, and J. Pérez-Ríos, Universal few-body physics and cluster formation, *Rev. Mod. Phys.* **89**, 035006 (2017).
- [34] A. Härter, A. Krüchow, M. Deiß, B. Drews, E. Tiemann, and J. H. Denschlag, Population distribution of product states following three-body recombination in an ultracold atomic gas, *Nat. Phys.* **9**, 512 (2013).
- [35] J. Wolf, M. Deiß, A. Krüchow, E. Tiemann, B. P. Ruzic, Y. Wang, J. P. D'Incao, P. S. Julienne, and J. H. Denschlag, State-to-state chemistry for three-body recombination in an ultracold rubidium gas, *Science* **358**, 921 (2017).
- [36] J. Wolf, M. Deiß, and J. Hecker Denschlag, Hyperfine Magnetic Substrate Resolved State-to-State Chemistry, *Phys. Rev. Lett.* **123**, 253401 (2019).
- [37] Y. Wang and P. S. Julienne, Universal van der Waals physics for three cold atoms near Feshbach resonances, *Nat. Phys.* **10**, 768 (2014).
- [38] K. Kato, Y. Wang, J. Kobayashi, P. S. Julienne, and S. Inouye, Isotopic Shift of Atom-Dimer Efimov Resonances in K-Rb Mixtures: Critical Effect of Multichannel Feshbach Physics, *Phys. Rev. Lett.* **118**, 163401 (2017).
- [39] R. Chapurin, X. Xie, M. J. Van de Graaff, J. S. Popowski, J. P. D'Incao, P. S. Julienne, J. Ye, and E. A. Cornell, Precision Test of the Limits to Universality in Few-Body Physics, *Phys. Rev. Lett.* **123**, 233402 (2019).
- [40] X. Xie, M. J. Van de Graaff, R. Chapurin, M. D. Frye, J. M. Hutson, J. P. D'Incao, P. S. Julienne, J. Ye, and E. A. Cornell, Observation of Efimov Universality Across a Nonuniversal Feshbach Resonance in ^{39}K , *Phys. Rev. Lett.* **125**, 243401 (2020).
- [41] T. Secker, J.-L. Li, P. M. A. Mestrom, and S. J. J. M. F. Kokkelmans, Multichannel nature of three-body recombination for ultracold ^{39}K , *Phys. Rev. A* **103**, 022825 (2021).
- [42] C. Chin, R. Grimm, P. Julienne, and E. Tiesinga, Feshbach resonances in ultracold gases, *Rev. Mod. Phys.* **82**, 1225 (2010).
- [43] E. O. Alt, P. Grassberger, and W. Sandhas, Reduction of the three-particle collision problem to multi-channel two-particle Lippmann-Schwinger equations, *Nucl. Phys. B* **2**, 167 (1967).
- [44] E. Braaten, H.-W. Hammer, D. Kang, and L. Platter, Three-body recombination of identical bosons with a large positive scattering length at nonzero temperature, *Phys. Rev. A* **78**, 043605 (2008).
- [45] P. M. A. Mestrom, T. Secker, R. M. Kroeze, and S. J. J. M. F. Kokkelmans, Finite-range effects in Efimov physics beyond the separable approximation, *Phys. Rev. A* **99**, 012702 (2019).
- [46] T. Secker, J.-L. Li, P. M. A. Mestrom, and S. J. J. M. F. Kokkelmans, Three-body recombination calculations with a two-body mapped grid method, *Phys. Rev. A* **103**, 032817 (2021).
- [47] Z. Shotan, O. Machtey, S. Kokkelmans, and L. Khaykovich, Three-Body Recombination at Vanishing Scattering Lengths in an Ultracold Bose Gas, *Phys. Rev. Lett.* **113**, 053202 (2014).
- [48] P. S. Julienne and J. M. Hutson, Contrasting the wide Feshbach resonances in ^6Li and ^7Li , *Phys. Rev. A* **89**, 052715 (2014).
- [49] One should not confuse $|\psi_{\text{scat}}\rangle_\alpha$ with the system's real initial state $|\psi_{\text{in}}\rangle$ describing three free atoms.
- [50] C. Strauss, T. Takekoshi, F. Lang, K. Winkler, R. Grimm, J. Hecker Denschlag, and E. Tiemann, Hyperfine, rotational, and vibrational structure of the $a^3\Sigma_u^+$ state of $^{87}\text{Rb}_2$, *Phys. Rev. A* **82**, 052514 (2010).

- [51] The small discrepancy between our calculated magnetic field value $B = 578$ G of this zero crossing and the value $B \approx 576$ G given by Ref. [47] comes from slight differences in the interaction potentials employed in both calculations. The effect of this discrepancy on the three-body recombination rate is negligible.
- [52] K. Giergiel, T. Tran, A. Zaheer, A. Singh, A. Sidorov, K. Sacha, and P. Hannaford, Creating big time crystals with ultracold atoms, *New J. Phys.* **22**, 085004 (2020).
- [53] L. Khaykovich, F. Schreck, G. Ferrari, T. Bourdel, J. Cubizolles, L. D. Carr, Y. Castin, and C. Salomon, Formation of a matter-wave bright soliton, *Science* **296**, 1290 (2002).
- [54] K. E. Strecker, G. B. Partridge, A. G. Truscott, and R. G. Hulet, Formation and propagation of matter-wave soliton trains, *Nature (London)* **417**, 150 (2002).
- [55] J. H. V. Nguyen, P. Dyke, D. Luo, B. A. Malomed, and R. G. Hulet, Collisions of matter-wave solitons, *Nat. Phys.* **10**, 918 (2014).
- [56] D. Luo, Y. Jin, J. H. V. Nguyen, B. A. Malomed, O. V. Marchukov, V. A. Yurovsky, V. Dunjko, M. Olshanii, and R. G. Hulet, Creation and Characterization of Matter-Wave Breathers, *Phys. Rev. Lett.* **125**, 183902 (2020).
- [57] C. Eigen, A. L. Gaunt, A. Suleymanzade, N. Navon, Z. Hadzibabic, and R. P. Smith, Observation of Weak Collapse in a Bose-Einstein Condensate, *Phys. Rev. X* **6**, 041058 (2016).
- [58] M. D. Lee, T. Köhler, and P. S. Julienne, Excited Thomas-Efimov levels in ultracold gases, *Phys. Rev. A* **76**, 012720 (2007).
- [59] D. J. Ernst, C. M. Shakin, and R. M. Thaler, Separable representations of two-body interactions, *Phys. Rev. C* **8**, 46 (1973).
- [60] L. Hlophe, Ch. Elster, R. C. Johnson, N. J. Upadhyay, F. M. Nunes, G. Arbanas, V. Eremenko, J. E. Escher, and I. J. Thompson (TORUS Collaboration), Separable representation of phenomenological optical potentials of Woods-Saxon type, *Phys. Rev. C* **88**, 064608 (2013).